ACSNANO

www.acsnano.org

ARTICLE

Monolithic Nanoporous Zn Anode for Rechargeable Alkaline Batteries

Congcheng Wang,[#] Guoyin Zhu,[#] Pan Liu, and Qing Chen*

Cite This: https://dx.doi.org/10.1021/acsnano.9b09669

Read Online

ACCESS | Metrics & More | Article Recommendations | Supporting Information

ABSTRACT: The fabrication of monolithic nanoporous zinc bears its significance in safe and inexpensive energy storage; it can provide the much needed electrical conductivity and specific area in a practical alkaline battery to extend the short cycle life of a zinc anode. Although this type of structure has been routinely fabricated by dealloying, that is, the selective dissolution of an alloy, it has not led to a rechargeable zinc anode largely because the need for more reactive metal as the dissolving component in dealloying limits the choices of alloy precursors. Here, we apply the mechanism of dealloying, percolation dissolution, to design a process of reduction-induced decomposition of a zinc compound ($ZnCl_2$) for nanoporous zinc. Using naphthalenide solution, we confine the selective dissolution of chloride to the compound/electrolyte interface, triggering the spontaneous formation of a network of 70 nm wide percolating zinc ligaments that retain the shape of a 200 μm thick monolith. We further reveal that this structure, when electrochemically oxidized and reduced in an alkaline electrolyte, undergoes surface-diffusion-controlled coarsening toward a quasi-steady-state with a length scale of ~500 nm. The coarsening dynamics preserves the continuous zinc phase, enabling its uniform reaction and 200 cycles of stable performance at 40% depth of discharge (328 mAh/g) in a Ni–Zn battery.

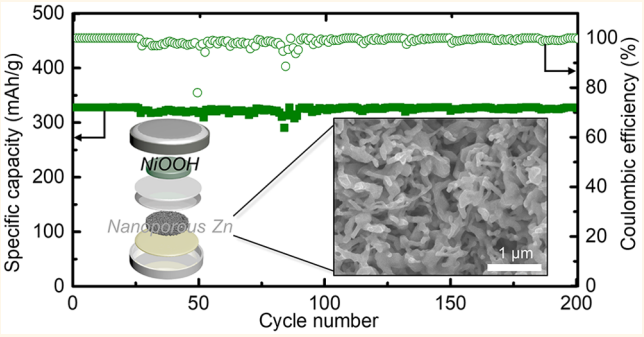

KEYWORDS: *nanoporous metal, zinc anode, dealloying, structural evolution, nickel–zinc battery*

Monolithic nanoporous metals, a class of material produced by dealloying (*i.e.*, the selective dissolution of a homogeneous alloy), grant us rare access to large metallic surface areas inside bulk materials.[1,2] The material comprises numerous small, curvy, but uniform metal ligaments and pores, evolving *via* a mechanism of percolation dissolution, an intuitive description of the complex interplay between surface kinetics and the selective dissolution. The word percolation applies to both the ligaments and pores given the sufficiently high concentrations of the dissolving and remaining components in the alloy precursor. The percolation of the pores sustains the rapid dissolution which could not otherwise occur *via* slow solid-state diffusion, and the percolation of the ligaments upholds the monolithic structure, inheriting the shape and the high conductivity from the alloy. We can thus fit the dealloyed materials into electrochemical devices easily and use the structures to tackle many grand challenges, including air cathodes for fuel cells,[3] electrochemical actuation,[4] and high-capacity electrodes for lithium-ion batteries.[5]

However, the success in applications is largely limited to nanoporous noble metals, whereas reactive metals have been less exploited. Not until very recently did researchers start to prepare nanoporous reactive metals such as Al,[6,7] Mg,[8] and Zn.[9] The underlying challenge is the fabrication of reactive metal through an oxidative process like dealloying, which requires a more reactive component to dissolve from the precursor. Take Zn for example. Among a handful of possible dissolving components, Li or Mg cannot form a homogeneous, single-phase alloy with Zn in a desirable compositional range. BaZn and CaZn alloys seem viable from the phase diagrams, but it is strenuous to prepare these extremely reactive alloys with high homogeneity and then dealloy them.

We are particularly interested in the fabrication of monolithic nanoporous Zn for a stable Zn battery. Zn, the anode of the Volta pile, continues to attract the attention of researchers and developers with its high capacity, global abundance, and compatibility with aqueous electrolytes. A Zn

Received: December 9, 2019
Accepted: February 4, 2020
Published: February 4, 2020

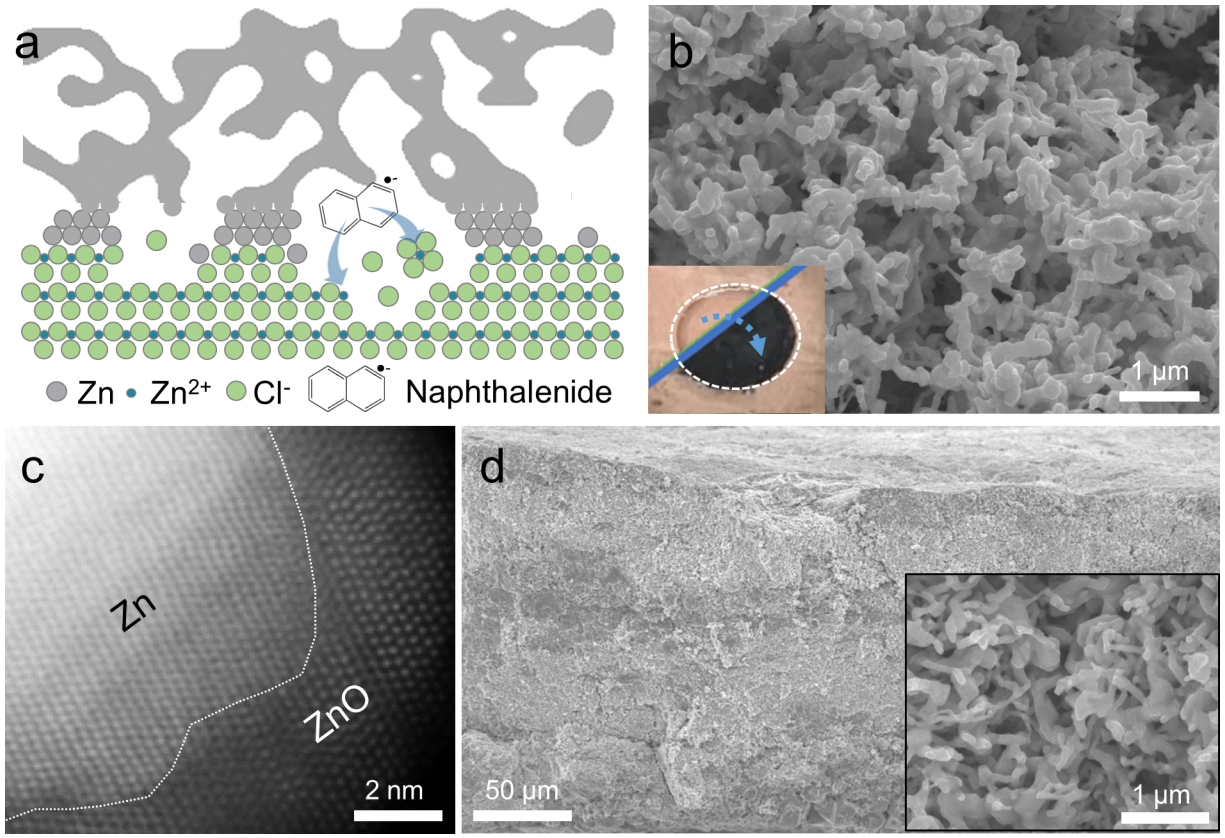

Figure 1. Fabrication of nanoporous Zn by RID. (a) Cartoons illustrating the mechanism of structural evolution. The mechanism assumes the solvated cation as one possible reaction intermediate, although the exact route of the reaction is beyond our knowledge. (b) SEM of the nanoporous Zn from RID, with an inset of photos showing the transformation of a transparent sheet of $ZnCl_2$ to dark black nanoporous Zn after RID (inside the white dashed circle). (c) HAADF-STEM image of a Zn ligament covered by a layer of ZnO. (d) Cross-sectional SEM of the nanoporous Zn after being compressed to a porosity of 75% (the inset is the same sample at a higher magnification).

anode can be coupled to an air cathode for a practical energy density up to 400 Wh/kg,[10] and it can also replace metal hydrides in a commercial alkaline cell for a low-cost Ni−Zn battery.[11] The Ni−Zn battery was attracting much attention in the late last century, but it did not overcome the competition from Li-ion batteries as the Zn anode suffers from a poor cycle life when pushed toward a high depth of discharge (DoD) for a high energy density. A conventional Zn anode, made from charging a ZnO powder electrode, faces issues of shape changes,[12] passivation,[13] and dendrite formation.[14] Although additives to the anode and the electrolyte were effective in partly alleviating the issues,[14] they have not stabilized the anode at a high DoD. Commercial cells have been falling short in providing consistent performance,[15] and new systems often dilute the energy density with flowing electrolytes for longer cycle lives.[16]

More recent studies have demonstrated the importance of having Zn metal in the anodes. Instead of using a sheet of Zn foil that passivates before delivering a high areal capacity, these anodes contain continuous phases of Zn at smaller length scales, which provides stable, uniform conductivity to promote a uniform distribution of reaction.[17,18] In particular, Parker *et al.* showed that a spongy Zn anode derived from Zn powder emulsion could deliver more than 100 cycles at 40% DoD.[19−21] Turney *et al.* demonstrated up to 1500 cycles at a shallow DoD with a Zn powder anode.[22] Nonetheless, Zn powder remains the main ingredient in the recipe, offering little space for structural design, which also limits our understanding of what makes a good Zn anode.[23]

In this work, we design a nanoporous Zn anode with the mechanism of percolation dissolution applied to a compound precursor to circumvent the limits from the alloys. The process, termed reduction-induced decomposition (RID), selectively dissolves chloride anions from a sheet of $ZnCl_2$, triggering the spontaneous formation of nanoporous Zn.[24] The as-fabricated monolithic nanoporous Zn provides not only a continuous Zn phase but also a stable, small length scale that enable it to deliver a high power output and 200 deep cycles in a Ni−Zn cell.

RESULTS AND DISCUSSION

Fabricating Nanoporous Zn *via* RID. We begin by describing the working mechanism of RID based on our understanding of percolation dissolution.[24,25] A typical half-reaction of RID goes as $M_mX_x + xm\,e^- \rightarrow mM + xX^{m-}$, where M_mX_x is the compound precursor, M the metal product, and e^- the electron from a reducing solution. Unlike most synthesis that dissolves a compound before reducing its metal cations to metal, RID takes a straight route from the compound to the metal. The metal phase will grow from the compound surface once in contact with a reducing solution, first as islands and then as curvy ligaments. With a sufficiently large molar volume change (ΔV^m), percolating pores will evolve spontaneously with the dissolution. Meanwhile, if ΔV^m is not too large, the metal ligaments, undergoing surface-diffusion-controlled coars-

https://dx.doi.org/10.1021/acsnano.9b09669
ACS Nano XXXX, XXX, XXX−XXX

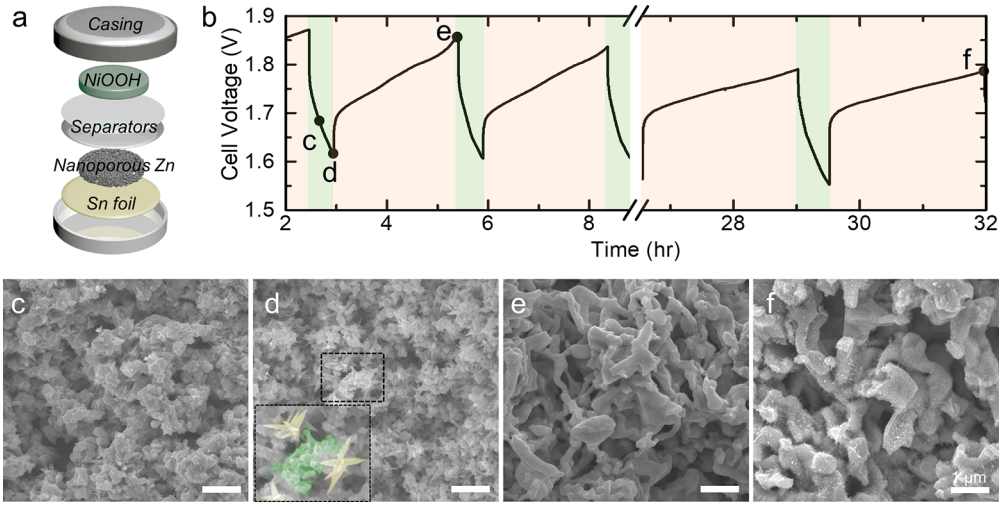

Figure 2. Structural evolution of the nanoporous Zn during discharging (oxidation) and charging (reduction) cycles. (a) Build of the Ni−Zn cell. (b) Voltage *vs* time curve of 10 cycles of discharging (green shaded) and charging (orange shaded). SEM of the anodes at 20% DoD in the first discharging (c), 40% DoD at the end of the first discharging (d), 0% DoD at the end of the second charging (e), and 0% DoD at the end of the 10th charging (f), corresponding to the black dots in (b). In (d), we highlight the ZnO flowers and the pits in the ligaments in pale white and green, respectively.

ening, will percolate to retain the shape of the compound. This scenario of percolation dissolution is summarized in Figure 1a.

The mechanism informs us of the following criteria for designing a RID reaction. We will need an insoluble M_mX_x, a sufficiently strong reductant, and a highly soluble anion X^{m-} to avoid passivation. The nucleation of the metal on M_mX_x requires low interfacial energy, that is, good wetting, which will also prevent the metal phase from easy detachment from the reacting compound precursor during coarsening. The bounds for ΔV^m can be approximated from continuum percolation theory[26] that suggests a volumetric threshold ($p_v \sim 14-16\%$) for a component to percolate in a random mixture. Therefore, the preferred range of ΔV^m is

$$p_v < \Delta V^m < 1 - p_v \quad (1)$$

so that under the assumption of no macroscopic volume change, RID can create continuous, open pores to sustain dissolution and a continuous metal phase to yield monolithic material.

With the above requirements in mind, we proceed with the fabrication of nanoporous Zn. A seemingly proper choice of a precursor is ZnO, given its low solubility in most solvents. However, in an aqueous solution, we could not identify a sufficiently strong reductant, and in a nonaqueous solution that can accommodate a stronger reductant, the oxide product had a hard time dissolving, leading to a superficial layer of Zn product even after half a day of reaction (Figure S1a). Similar issues occurred if we used ZnS as the precursor (Figure S1b). Therefore, we turned to another common Zn salt, $ZnCl_2$. In dimethoxyethane (DME), $ZnCl_2$ is sparingly soluble, whereas its RID product, Cl^-, can readily dissolve with Li^+ as the supporting cation in the solution. ΔV^m for the conversion of $ZnCl_2$ to Zn is 80.5%, falling in the desirable range. The wetting angle between Zn and $ZnCl_2$ is about 25° (Figure S2a), making the surface of $ZnCl_2$ a favored site for Zn nucleation.

The RID experiment is designed as follows. The reductant, naphthalenide, has a relatively short lifetime, so it has to be prepared right before RID by reacting naphthalene with a sheet of Li foil. Li here serves as a convenient source of electrons, although in the future, the oxidation of the solvent in an electrolyzer would make more economic sense at scale. The formation of naphthalenide gave the solution a deep green color, as shown in Figure S2b. The polycrystalline $ZnCl_2$ precursor was prepared in the form of a disk by melting $ZnCl_2$ powder in a copper crucible (the inset of Figure 1b). The $ZnCl_2$ sample, together with the crucible, was then immersed in the reducing solution for ~3 h. After the reaction, the transparent $ZnCl_2$ disk turned black without losing its integrity (the inset of Figure 1b). Although the sample is brittle, the strength suffices the handling during characterization and later battery assembling, as shown by Figure S2c.

The scanning electron microscopy (SEM) image in Figure 1b shows the cross-sectional morphology of the product, a nanoporous structure with slim ligaments. We confirmed the bulk composition of the ligaments to be pure Zn with energy-dispersive spectroscopy (EDS, Figure S3a) and X-ray diffraction (XRD, Figure S3b). The randomly oriented metal ligaments have an average width of around 67 nm (statistics of the ligament width shown in a histogram in Figure S4), smaller than our expectation given much larger ligaments observed for other nanoporous base metals such as Pb and Sn.[25,27] We attribute this small length scale to two factors. The first is the electrolyte environment where the structure evolved. Surface diffusion of metal in an organic electrolyte can be slower than that in water, which can be further slowed down by a salt layer on the Zn surface formed during the reaction (Figure S2d).[27] The second factor is the formation of surface oxide likely during the step of cleaning with ethanol, as confirmed by high-angle annular dark-field scanning transmission electron microscopy (HAADF-STEM, Figure 1c). The lattice spacings and the diffraction patterns of the two phases (Figure S5a,b) confirm that a thin, compact layer of ZnO covers the Zn ligament uniformly despite its high curvature. The thickness of the ZnO layer in Figure 1c is around 2.9 nm. The interface between Zn and ZnO appears semicoherent, with the lattice mismatch accommodated by dislocations (Figure S5c).

https://dx.doi.org/10.1021/acsnano.9b09669
ACS Nano XXXX, XXX, XXX−XXX

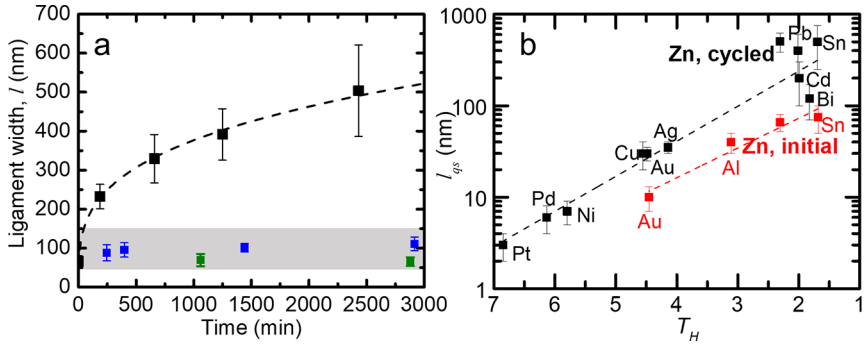

Figure 3. Length scale evolution of the nanoporous Zn during cycling. (a) Ligament width *vs* time in the cycling cell (black squares, fitted to the dashed line with an exponent of 0.297). The changes in ligament width in 6 M KOH saturated with ZnO (blue squares) and argon (green squares) are shown for comparison. The shaded region highlights the length scale at which the electrochemical reactions can act to reshape the anode. (b) Summary of l_{qs} *vs* T_H for nanoporous metals fabricated in aqueous solutions (black) and ether-based organic solutions (red). References and discussion on the analysis can be found in the Supporting Information.

The nanoporous Zn inherits a large porosity from the large ΔV^m, which can be too big to effectively serve as an anode given the expected decrease in ligament connectivity upon discharging.[19] The porosity was estimated by measuring the dimensional changes of the sample, given ΔV^m as the theoretical porosity with no volume change. The as-prepared porosity is above 80%.[24] To tune down the porosity, the most common method is to change the precursor,[24] which will require another round of reaction design. An alternative approach is mechanical compression. Figure 1d shows the cross-sectional structure of the nanoporous Zn after being compressed at 6.8 MPa to a porosity of 75%. The deformation was rather uniform, likely owing to the structural uniformity. This specific value of porosity ensures large pore space for mass transports and a high enough volume of metal for electrical conduction, even when it undergoes deep discharging. For example, at 40% DoD and assuming no overall volume change of the electrode, the porosity decreases to ~69% given that the density of ZnO is lower than that of Zn, but this porosity is still higher than a typical value of a porous anode.[28] The volume fraction of Zn decreases from 25 to 16%, close to p_v for a percolating Zn phase.

Structural Evolution of the Nanoporous Zn as an Anode. Before engaging cycling experiments of the nanoporous Zn, we take advantage of its uniformity to investigate the structural evolution of a nanostructured Zn anode, a rarely studied but critical factor underlying the cycling stability. We carried out a series of *ex situ* microscopic characterizations to capture structural changes step by step in discharging and charging processes. The electrochemical tests were performed in a coin cell, comprising an oversized NiOOH cathode, an electrolyte of 6 M KOH saturated with ZnO, and other commercial cell components (Figure 2a). We did not use a symmetric cell with two nanoporous zinc electrodes, as the anode reactions do not require a balance in zincate ions. Instead, the oversized NiOOH cathode allows us to conveniently reach various DoD values and investigate the electrochemical behaviors of the anode. A characteristic curve of voltage *versus* time is shown in Figure 2b, with a discharging current of 25 mA/cm^2 and a charging current of 5 mA/cm^2. No voltage hold was necessary in charging given the oversized cathode. We stopped the cycling tests of different cells at different stages (black dots in Figure 2b) and retrieved the anodes for SEM characterization.

The nanoporous Zn anode experienced significant structural changes but retained the uniform, percolating ligaments, as shown in Figure 2c–f. The ligaments became rougher when discharged to 20% DoD, and the roughness developed into a seemingly secondary porosity at 40% DoD, as a result of both Zn dissolution and ZnO formation. Highlighted in the inset of Figure 2d, the dissolution grows ZnO flowers alongside with pits in the ligaments. The pits and the flowers reside closely, but they can be told apart even at the end of discharging, which we believe is key to stabilizing the structure. If the two are far apart spatially, zincate sequestration and ZnO formation must be sluggish, and shape changes would eventually damage the structure. On the contrary, if the two overlap spatially, passivation would take place to prevent deep discharging. Upon recharging, the electrode was able to return to the nanoporous metal structure (Figure 2e). The metal network is upheld throughout the cycling, as also suggested by stable high-frequency impedance measured *via* electrochemical impedance spectroscopy (EIS, Figure S6a).

Through 10 repetitive cycles, the Zn anode remained nanoporous (Figure 2f), but the length scale (*i.e.* the widths of ligaments and pores) increased. The increase was rapid in the first few cycles, but it then slowed down, apparent from Figure 3a, showing a plot of the ligament width l *versus* the total time t spent in the cell (statistics of the ligament widths can be found in Figure S4). In the same plot, we show that nanoporous Zn kept in argon (blue dots) and a ZnO-saturated KOH electrolyte (green dots) for a similar period showed much smaller changes. If replotted at a logarithmic scale, the curve of $ln(l)$ and $ln(t)$ shows a slope of ~0.297. This value is close to a quarter and even closer to the scaling exponent estimated from the isothermal coarsening of nanoporous metals,[29] suggesting surface-diffusion-controlled coarsening. The length scale change can thus be mathematically described as follows:[30]

$$l^4 - l_0^4 = \frac{\gamma a^4 D_s t}{kT} \quad (2)$$

where l_0 is the initial ligament width, γ the surface energy, a the lattice constant, D_s the surface diffusivity, k the Boltzmann constant, and T the experimental temperature. When l_0 is significantly smaller than the change in l, as in the case of the cycled nanoporous Zn, l becomes linearly dependent on $t^{1/4}$. This relationship implies a quasi-steady-state ligament width (l_{qs}) reached within a typical experimental period of days,

https://dx.doi.org/10.1021/acsnano.9b09669
ACS Nano XXXX, XXX, XXX−XXX

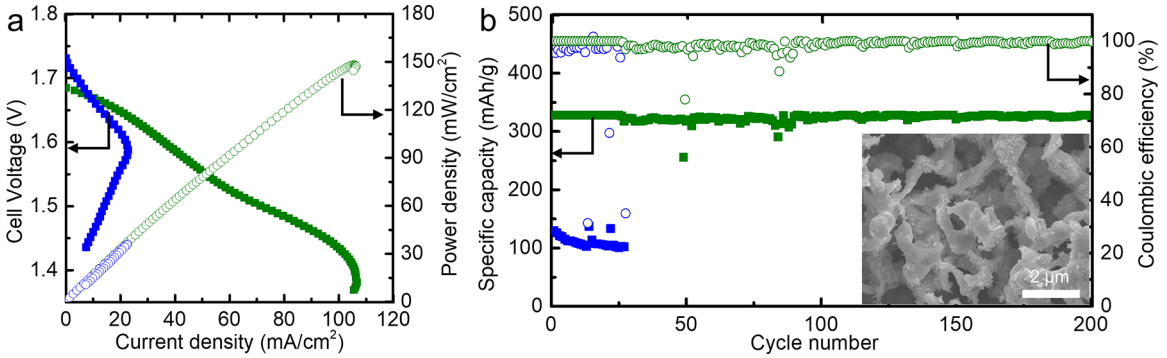

Figure 4. Performance of the nanoporous Zn anode in a Ni−Zn battery. (a) Cell voltages (solid squares) and power densities (circles) *vs* current densities from the polarization tests of the nanoporous Zn (green) and the Zn powder anode (blue). (b) Capacity (solid squares) and Coulombic efficiencies (circles) for the two with the same color coding. The inset is the cross-sectional SEM of the nanoporous Zn anode after 200 cycles.

which does not grow significantly for a much longer periods (see discussion in the Supporting Information).

As the mechanism behind the coarsening would eventually determine the cycling stability of the nanoporous Zn, we carry out the following analysis to further understand how the change of length scales may depend on time and environment. We first focus on D_s, the only material property in eq 2 that depends strongly on the environment. The biggest difference between the nanoporous Zn cycled in the cell and kept in argon is the surface ZnO layer. In the cycling cell, particularly during charging, the layer would be gone, leaving "naked" Zn ligaments to coarsen at a rate more characteristic of metallic Zn in an aqueous solution. The explanation can be supported by the relationship between l and the homologous temperature (T_H). T_H, a metallurgical term used to predict creep, manifests the empirical proportionality between the activation energy of surface diffusion and the melting point, as both relate to the binding energy.[31] We can derive from eq 2 the following relationship between l_{qs} and T_H:

$$\log l_{qs} = \frac{1}{4}\log\left(\frac{\gamma a^4 D_{s,0} t}{kT}\right) - \frac{\alpha T_H}{4} \tag{3}$$

where $D_{s,0}$ is the maximum surface diffusivity and α is a constant (see Supporting Information for details of the derivation). Although it is crude to assume the first term on the right-hand side of eq 3 to be a constant, a linear relationship between $\log(l_{qs})$ and T_H has been previously shown for many nanoporous metals from aqueous dealloying, replotted as black dots in Figure 3b.[27,32] The cycled Zn anode resides nearby. The small initial l of the nanoporous Zn, alongside literature values on dealloying in ether-based solutions, makes another line right below their aqueous counterparts. Both ligament widths of the nanoporous Zn are thus quasi-steady-states, with their difference from the different surface diffusivities in aqueous and nonaqueous solutions.

We believe that the above coarsening dynamics, though lowering the specific area, can play important roles in the structural stability. The most obvious benefit is the morphological retention despite the length scale change, a phenomenon commonly observed when surface diffusion acts on nanoporous metals.[33] It preserves the continuous metal phase, one most needed characteristic for a Zn anode. The second structural outcome is the quasi-steady-state length scale of ~500 nm. To coarsen it further by a factor of 2, it would take ~160 more cycles, which is already an appreciable cycle life for a Zn anode. Last but not least, surface diffusion may have held off another structure-altering dynamics, the electrochemical reaction. We may understand their interplay through the length scales at which they operate. Two notable length scales associated with the reaction are the size and interspacing of the ZnO flowers, both around 100 nm (the shaded area in Figure 3a). This length scale is likely how far the diffusion of zincates can relocate Zn mass. If the ligaments remained ~70 nm wide, the repetitive dissolution could have either cut them off or induced solid-state Plateau−Rayleigh instability to reshape ligaments into particles as the structural perturbation is larger than the ligament diameter.[34] Fortunately, surface diffusion acts quickly to enlarge the ligaments beyond 100 nm and continues to counter any roughening at a similar scale.

Stable Ni−Zn Battery with a Nanoporous Zn Anode. The structural stability promises stable cycling performance, which was indeed achieved in a Ni−Zn battery. We stick to the Ni−Zn chemistry here instead of exploring emerging Zn-ion batteries,[35] as the plating and stripping reactions in a neutral electrolyte would destroy the nanoporous structure. The battery was assembled similarly to that in Figure 2a, but with tighter control over the electrolyte volume, whose zincate contributes less than 10% of the overall Zn mass to the cell. This control is to make the test more practically relevant, as advocated by many previous studies.[22,36] We did not include any additives in the electrode or the electrolyte, so that the test may reflect the genuine performance of the nanoporous Zn. For comparison, we made an anode from Zn powder (~150 μm in diameter) and tested it under a similar condition. The cells were discharged to 40% DoD (or a voltage cutoff of 1.35 V) at 25 mA/cm^2 and fully charged (or to 1.9 V) at 5 mA/cm^2, with no voltage hold or conditioning cycles.

Before cycling, we ran polarization tests (Figure 4a), which show a much higher discharging current and power density from the cell with the nanoporous Zn anode. The curve started at a lower open-circuit voltage for the nanoporous Zn as it began with a degree of oxidation higher than that of the Zn powder anode. The powder anode suffers a rapid loss of cell voltage as we ramped up the current density. The large difference in polarization likely originates from two structural differences as we have been highlighting in the work. The first is the high and stable conductivity of the nanoporous Zn, and the second is its high specific area that offers more sites for

https://dx.doi.org/10.1021/acsnano.9b09669
ACS Nano XXXX, XXX, XXX−XXX

charge transfer. The discharging current peaks at ~100 mA/cm^2 for the nanoporous Zn, which is likely a result of both mass transport limits and passivation. Nevertheless, it delivers a peak power over 150 mW/cm^2, 4 times higher than that from the Zn powder anode.

Figure 4b plots the discharging capacities against the number of cycles, showing the stable performance of the nanoporous Zn anode. During the 12 day test, the anode consistently delivered a capacity ~328 mAh/g, 40% of the theoretical value. The corresponding areal capacity is 5.7 mAh/cm^2. The Coulombic efficiency is, on average, 98.8%, much higher than that of a typical Ni–Zn battery,[15] as the conductive anode and the oversized cathode helped suppress hydrogen and oxygen evolutions, respectively. The high specific area of the nanoporous Zn did not seem to provoke severe hydrogen evolution, although in a practical cell where the cathode limits capacity, we may need additives to further improve the Coulombic efficiency. The energy efficiency was ~87.6%; the loss likely came from the ionic resistances through two separators and the thick electrodes (Figure S6b). In comparison, the Zn powder electrode could not even reach 40% DoD due to severe polarization in discharging, and its Coulombic efficiency quickly decreased as it reached the 25th cycle, where we suspect that dendrites killed the cell. The capacity delivered by the nanoporous anode can translate roughly to an energy density of 110 Wh/kg in a practical Ni–Zn battery if we assume that a capacity-limiting cathode and the Zn anode make up ~39% of the weight.[20] This performance stands out, particularly among Zn anodes discharged to a high DoD (Table S1).

The structural stability is corroborated by post mortem microscopic characterization. The inset of Figure 4b shows the structure of the anode retrieved at the end of the 200th cycle (a lower magnification image can be found in Figure S8). The anode, though fragile, retains its integrity. We did not notice any dendrite on the surface of the anode or the separators. The nanoporous structure prevails in the anode. The ligament width stays around 500 nm, but the pores are visibly larger. The cross section appears less uniform with big holes. These structural changes, along with the fragility and the increased cell impedance (Figure S6b) suggest a possible loss in Zn mass, which is difficult to avoid given the strong tendency of zincate to supersaturate this electrolyte.[37] Nonetheless, the Zn network in the electrode overcomes 200 deep cycles, which promises highly rechargeable Zn batteries to be fulfilled by future engineering.

CONCLUSIONS

RID circumvents the limits by alloy precursors in dealloying and broadens the path toward functional nanoporous structures. The use of nonaqueous solution for RID will enable more choices of insoluble precursors, particularly for the fabrication of nanoporous reactive metals. We demonstrate the application of one such structure in a rechargeable Zn battery. The nanoporous Zn from RID delivered outstanding performance under a practical cycling condition, owing to the structural stability and the large specific area. The results also underscore the dependence of cycling stability on microstructural evolution, a poorly understood topic even for the grand old Zn anode. The nanoporous Zn, with its compositional and structural uniformity and tunability, provides a model system for building structure–property relationships and a starting point for electrode and electrolyte engineering to realize safe and inexpensive Zn batteries.

METHODS

Material Fabrication. $ZnCl_2$ precursor (0.8 cm^2 in size) was prepared by melting $ZnCl_2$ (J&K Scientific) powder in a copper crucible at 400 °C. To prepare lithium naphthalenide solution, a fresh-cut lithium sheet (Shenzhen Teensky Technology Co., Ltd.) was put into an anhydrous dimethoxyethane (J&K Scientific) solution of 0.5 M naphthalene (J&K Scientific) and 0.1 M $LiPF_6$ (TCI). The solution was stirred at room temperature in a glovebox until the lithium was completely dissolved. RID experiments were performed by immersing the precursor into the solution for 3 h. After RID, the sample was thoroughly washed in sequence with anhydrous dimethoxyethane and anhydrous ethanol (J&K Scientific). RID of ZnO and ZnS sheets (Beijing Special Ceramic Hyflux Ltd.) was carried out similarly, except that they were immersed in lithium naphthalenide solution for 12 h.

Material Characterization. SEM and EDS characterization were both performed with a JEOL-7100F scanning electron microscope. All images are from cross sections. For the estimate of ligament width, we measured 30 ligaments per sample. Anodes harvested from cycled cells were rinsed with acetone (Scharlau) to remove residual salts and then dried and stored under vacuum before characterization.

STEM characterization was performed in a cold field-emission transmission electron microscope (JEOL ARM200F, 200 keV) with spherical aberration corrector for the probe-forming lenses, which was operated at 200 kV. The Cs corrector was optimized for STEM observations, and the point-to-point resolution in the STEM mode is better than 1.0 Å. For HAADF-STEM imaging, the electron probe convergence angle of 25 mrad and an HAADF detector with an inner angle larger than 100 mrad were used. The HAADF detector was set to collect electrons scattered between 100 and 267 mrad, guaranteeing that the collected signals give an approximately incoherent atomic number contrast in HAADF-STEM.

XRD characterization was conducted using a model PW1830 (Philips) X-ray diffractometer with Cu Kα radiation (λ = 1.5406 Å) in a scan range (2θ) of 10–80°.

Battery Assembly and Testing. Ni–Zn batteries were assembled into coin-type cells (CR2032) with a Zn anode, either the compressed nanoporous Zn (~0.36 cm^2 in size) or a pasted electrode comprising Zn powder (90 wt %, Aldrich), polyvinylidene fluoride (Arkema Kynar), and a NiOOH cathode (650 mAh, GP Batteries). Tin foil was used as the anode current collector. The anode was separated from the cathode by a nonwoven cellulose membrane and a microporous separator (Celgard 3501). A solution of 6.0 M KOH (VWR) saturated with ZnO (J&K Scientific) was used as the electrolyte. The electrolyte volume was controlled to be around 0.3 mL. The cells were assembled under a pressure of 6.8 MPa with an MSK-110 hydraulic coin cell crimper (Hefei Kejing Materials Technology Co. Ltd.). Cycling tests were performed with a Neware battery testing station (CT-3008W), with a charge and discharge current density of 5 and 25 mA/cm^2, respectively. Voltage cutoffs were set at 1.35 and 1.9 V, respectively. EIS was carried out with a Biologic VMP3 potentiostat, with a frequency range from 10 mHz to 7 MHz. The polarization tests were performed to a freshly assembled cell at a scan rate of 1 mV/s.

ASSOCIATED CONTENT

Supporting Information

The Supporting Information is available free of charge at https://pubs.acs.org/doi/10.1021/acsnano.9b09669.

Additional characterizations of structures from RID; EIS of the nanoporous Zn anode; derivation of the relationship between l_{qs} and T_H; comparison of cycling performance of Zn anodes in literature; and characterization of the nanoporous Zn anode after 200 cycles (PDF)

https://dx.doi.org/10.1021/acsnano.9b09669
ACS Nano XXXX, XXX, XXX–XXX

AUTHOR INFORMATION

Corresponding Author

Qing Chen − *Department of Mechanical and Aerospace Engineering, The Energy Institute, and Department of Chemistry, The Hong Kong University of Science and Technology, Kowloon, Hong Kong;* orcid.org/0000-0003-3106-9281; Email: chenqing@ust.hk

Authors

Congcheng Wang − *Department of Mechanical and Aerospace Engineering, The Hong Kong University of Science and Technology, Kowloon, Hong Kong*

Guoyin Zhu − *Department of Mechanical and Aerospace Engineering and Institute of Advanced Studies, The Hong Kong University of Science and Technology, Kowloon, Hong Kong*

Pan Liu − *State Key Laboratory of Metal Matrix Composites, and Shanghai Key Laboratory of Advanced High-temperature Materials and Precision Forming, School of Materials Science and Engineering, Shanghai Jiao Tong University, Shanghai 200240, China;* orcid.org/0000-0002-4063-9605

Complete contact information is available at: https://pubs.acs.org/10.1021/acsnano.9b09669

Author Contributions

#C.W. and G.Z. contributed equally.

Notes

The authors declare no competing financial interest.

ACKNOWLEDGMENTS

The work is fully supported by a grant from the Research Grants Council of the Hong Kong Special Administrative Region, China (T23-601/17-R). We also thank GP Batteries for providing battery materials.

REFERENCES

(1) McCue, I.; Benn, E.; Gaskey, B.; Erlebacher, J. Dealloying and Dealloyed Materials. *Annu. Rev. Mater. Res.* **2016**, *46*, 263−286.

(2) Weissmüller, J.; Sieradzki, K. Dealloyed Nanoporous Materials with Interface-Controlled Behavior. *MRS Bull.* **2018**, *43*, 14−19.

(3) Ding, Y.; Chen, M. Nanoporous Metals for Catalytic and Optical Applications. *MRS Bull.* **2009**, *34*, 569−576.

(4) Jin, H.-J.; Weissmuller, J. A Material with Electrically Tunable Strength and Flow Stress. *Science* **2011**, *332*, 1179−1182.

(5) Chen, Q.; Ding, Y.; Chen, M. Nanoporous Metal by Dealloying for Electrochemical Energy Conversion and Storage. *MRS Bull.* **2018**, *43*, 43−48.

(6) Yang, W.; Zheng, X.-G.; Wang, S.-G.; Jin, H.-J. Nanoporous Aluminum by Galvanic Replacement: Dealloying and Inward-Growth Plating. *J. Electrochem. Soc.* **2018**, *165*, C492−C496.

(7) Corsi, J. S.; Fu, J.; Wang, Z.; Lee, T.; Ng, A. K.; Detsi, E. Hierarchical Bulk Nanoporous Aluminum for On-Site Generation of Hydrogen by Hydrolysis in Pure Water and Combustion of Solid Fuels. *ACS Sustainable Chem. Eng.* **2019**, *7*, 11194−11204.

(8) Okulov, I. V.; Lamaka, S. V.; Wada, T.; Yubuta, K.; Zheludkevich, M. L.; Weissmüller, J.; Markmann, J.; Kato, H. Nanoporous Magnesium. *Nano Res.* **2018**, *11*, 6428−6435.

(9) Fu, J.; Deng, Z.; Lee, T.; Corsi, J. S.; Wang, Z.; Zhang, D.; Detsi, E. PH-Controlled Dealloying Route to Hierarchical Bulk Nanoporous Zn Derived from Metastable Alloy for Hydrogen Generation by Hydrolysis of Zn in Neutral Water. *ACS Appl. Energy Mater.* **2018**, *1*, 3198−3205.

(10) Fu, J.; Liang, R.; Liu, G.; Yu, A.; Bai, Z.; Yang, L.; Chen, Z. Recent Progress in Electrically Rechargeable Zinc−Air Batteries. *Adv. Mater.* **2019**, *31*, 1805230.

(11) McBreen, J. Nickel/Zinc Batteries. *J. Power Sources* **1994**, *51*, 37−44.

(12) Choi, K. W.; Bennion, D. N.; Newman, J. Engineering Analysis of Shape Change in Zinc Secondary Electrodes. *J. Electrochem. Soc.* **1976**, *123*, 1616−1627.

(13) Horn, Q. C.; Shao-Horn, Y. Morphology and Spatial Distribution of ZnO Formed in Discharged Alkaline Zn/MnO2 AA Cells. *J. Electrochem. Soc.* **2003**, *150*, A652−A658.

(14) Bass, K.; Mitchell, P. J.; Wilcox, G. D.; Smith, J. Methods for the Reduction of Shape Change and Dendritic Growth in Zinc-Based Secondary Cells. *J. Power Sources* **1991**, *35*, 333−351.

(15) Bonnick, P.; Dahn, J. R. A Simple Coin Cell Design for Testing Rechargeable Zinc-Air or Alkaline Battery Systems. *J. Electrochem. Soc.* **2012**, *159*, A981−A989.

(16) Ito, Y.; Nyce, M.; Plivelich, R.; Klein, M.; Steingart, D.; Banerjee, S. Zinc Morphology in Zinc−Nickel Flow Assisted Batteries and Impact on Performance. *J. Power Sources* **2011**, *196*, 2340−2345.

(17) Chamoun, M.; Hertzberg, B. J.; Gupta, T.; Davies, D.; Bhadra, S.; Van Tassell, B.; Erdonmez, C.; Steingart, D. A. Hyper-Dendritic Nanoporous Zinc Foam Anodes. *NPG Asia Mater.* **2015**, *7*, No. e178.

(18) Yan, Z.; Wang, E.; Jiang, L.; Sun, G. Superior Cycling Stability and High Rate Capability of Three-Dimensional Zn/Cu Foam Electrodes for Zinc-Based Alkaline Batteries. *RSC Adv.* **2015**, *5*, 83781−83787.

(19) Ko, J. S.; Geltmacher, A. B.; Hopkins, B. J.; Rolison, D. R.; Long, J. W.; Parker, J. F. Robust 3D Zn Sponges Enable High-Power, Energy-Dense Alkaline Batteries. *ACS Appl. Energy Mater.* **2019**, *2*, 212−216.

(20) Parker, J. F.; Chervin, C. N.; Pala, I. R.; Machler, M.; Burz, M. F.; Long, J. W.; Rolison, D. R. Rechargeable Nickel−3D Zinc Batteries: An Energy-Dense, Safer Alternative to Lithium-Ion. *Science* **2017**, *356*, 415−418.

(21) Parker, J. F.; Chervin, C. N.; Nelson, E. S.; Rolison, D. R.; Long, J. W. Wiring Zinc in Three Dimensions Re-Writes Battery Performance—Dendrite-Free Cycling. *Energy Environ. Sci.* **2014**, *7*, 1117−1124.

(22) Turney, D. E.; Gallaway, J. W.; Yadav, G. G.; Ramirez, R.; Nyce, M.; Banerjee, S.; Chen-Wiegart, Y. K.; Wang, J.; D'Ambrose, M. J.; Kolhekar, S.; Huang, J.; Wei, X. Rechargeable Zinc Alkaline Anodes for Long-Cycle Energy Storage. *Chem. Mater.* **2017**, *29*, 4819−4832.

(23) Stock, D.; Dongmo, S.; Janek, J.; Schröder, D. Benchmarking Anode Concepts: The Future of Electrically Rechargeable Zinc−Air Batteries. *ACS Energy Lett.* **2019**, *4*, 1287−1300.

(24) Wang, C.; Chen, Q. Reduction-Induced Decomposition: Spontaneous Formation of Monolithic Nanoporous Metals of Tunable Structural Hierarchy and Porosity. *Chem. Mater.* **2018**, *30*, 3894−3900.

(25) Chen, Q. Bi-Continuous Nanoporous Structure Formation *via* Compound Decomposition. *J. Electrochem. Soc.* **2014**, *161*, H643−H646.

(26) Zallen, R. *The Physics of Amorphous Solids*, 1st ed.; John Wiley & Sons: New York, 1983; pp 183−190.

(27) Chen, Q.; Sieradzki, K. Spontaneous Evolution of Bicontinuous Nanostructures in Dealloyed Li-Based Systems. *Nat. Mater.* **2013**, *12*, 1102−1106.

(28) Winter, M.; Brodd, R. J. What Are Batteries, Fuel Cells, and Supercapacitors? *Chem. Rev.* **2004**, *104*, 4245−4270.

(29) Qian, L. H.; Chen, M. W. Ultrafine Nanoporous Gold by Low-Temperature Dealloying and Kinetics of Nanopore Formation. *Appl. Phys. Lett.* **2007**, *91*, 083105.

(30) Mullins, W. W. Flattening of a Nearly Plane Solid Surface Due to Capillarity. *J. Appl. Phys.* **1959**, *30*, 77−83.

(31) Dalton, A. S.; Seebauer, E. G. An Improved Theory for Temperature-Dependent Arrhenius Parameters in Mesoscale Surface Diffusion. *Surf. Sci.* **2007**, *601*, 728−734.

(32) McCue, I.; Karma, A.; Erlebacher, J. Pattern Formation during Electrochemical and Liquid Metal Dealloying. *MRS Bull.* **2018**, *43*, 27−34.

https://dx.doi.org/10.1021/acsnano.9b09669
ACS Nano XXXX, XXX, XXX−XXX

(33) Lilleodden, E. T.; Voorhees, P. W. On the Topological, Morphological, and Microstructural Characterization of Nanoporous Metals. *MRS Bull.* **2018**, *43*, 20−26.
(34) Mullins, W. W.; Nichols, F. A. Surface- (Interface-) and Volume-Diffusion Contributions to Morphological Changes Driven by Capillarity. *Trans. Metall. Soc. AIME* **1965**, *233*, 1840−1847.
(35) Fang, G.; Zhou, J.; Pan, A.; Liang, S. Recent Advances in Aqueous Zinc-Ion Batteries. *ACS Energy Lett.* **2018**, *3*, 2480−2501.
(36) Zhang, Y.; Wu, Y.; Ding, H.; Yan, Y.; Zhou, Z.; Ding, Y.; Liu, N. Sealing ZnO Nanorods for Deeply Rechargeable High-Energy Aqueous Battery Anodes. *Nano Energy* **2018**, *53*, 666−674.
(37) Debiemme-Chouvy, C.; Vedel, J. Supersaturated Zincate Solutions: A Study of the Decomposition Kinetics. *J. Electrochem. Soc.* **1991**, *138*, 2538−2542.

https://dx.doi.org/10.1021/acsnano.9b09669
ACS Nano XXXX, XXX, XXX−XXX